

Accepted Manuscript

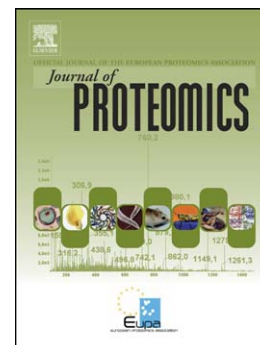
Profiling and identification of new proteins involved in brain ischemia using MALDI-imaging-mass-spectrometry

Víctor Llombart, Sebastián Alejandro Trejo, Sílvia Bronsoms, Anna Morancho, Ma Feifei, Júlia Faura, Teresa García-Berrocso, Alba Simats, Anna Rosell, Francesc Canals, Mar Hernández-Guillamón, Joan Montaner

PII: S1874-3919(16)30481-X
DOI: doi:[10.1016/j.jprot.2016.11.014](https://doi.org/10.1016/j.jprot.2016.11.014)
Reference: JPROT 2720

To appear in: *Journal of Proteomics*

Received date: 2 June 2016
Revised date: 24 October 2016
Accepted date: 19 November 2016



Please cite this article as: Llombart Víctor, Trejo Sebastián Alejandro, Bronsoms Sílvia, Morancho Anna, Feifei Ma, Faura Júlia, García-Berrocso Teresa, Simats Alba, Rosell Anna, Canals Francesc, Hernández-Guillamón Mar, Montaner Joan, Profiling and identification of new proteins involved in brain ischemia using MALDI-imaging-mass-spectrometry, *Journal of Proteomics* (2016), doi:[10.1016/j.jprot.2016.11.014](https://doi.org/10.1016/j.jprot.2016.11.014)

This is a PDF file of an unedited manuscript that has been accepted for publication. As a service to our customers we are providing this early version of the manuscript. The manuscript will undergo copyediting, typesetting, and review of the resulting proof before it is published in its final form. Please note that during the production process errors may be discovered which could affect the content, and all legal disclaimers that apply to the journal pertain.

Profiling and identification of new proteins involved in brain ischemia using MALDI-imaging-mass-spectrometry

Víctor Llombart¹, Sebastián Alejandro Trejo^{2,3}, Sílvia Bronsoms³, Anna Morancho¹, Ma Feifei¹, Júlia Faura¹, Teresa García-Berrocso¹, Alba Simats¹, Anna Rosell¹, Francesc Canals⁴, Mar Hernández-Guillamón¹, Joan Montaner¹

- 1- Universitat Autònoma de Barcelona, Neurovascular Research Laboratory, Institut de Recerca Vall d'Hebron, Barcelona, Spain
- 2- Instituto Multidisciplinario de Biología Celular (IMBICE), CONICET (Argentina).
- 3- Universitat Autònoma de Barcelona, Structural Biology and Proteomics Service, Barcelona, Spain.
- 4- Proteomics Laboratory, Vall d'Hebrón Institute of Oncology, Barcelona, Spain

KEYWORDS: MALDI-imaging, cerebral ischemia, tMCAO, ischemic stroke, biomarkers.

Corresponding author: Dr. Joan Montaner, Neurovascular Research Laboratory, Vall d'Hebron Institute of Research (VHIR), Vall d'Hebron University Hospital, Pg. Vall d'Hebron 119-129, 08035, Barcelona, Spain. +34 93 489 40 73, montaner.villalonga@gmail.com

Author's e-mail addresses: V. L. (llombs@hotmail.com), S. T. (sebatrejo@gmail.com), S. B. (Silvia.Bronsoms@uab.cat), A. M. (annamorancho@gmail.com), M. F. (mafeifeivhir@hotmail.com), J. F. (juliafaura10@gmail.com), T. G-B. (teresa.garcib@gmail.com), A. S. (alba.simats@vhir.org), A. R. (anna.rosell@gmail.com), F. C. (fcanals@vhio.net), M. H-G. (marguillamon@gmail.com), J. M. (montaner.villalonga@gmail.com).

Supporting information:

- Supplemental table SI
- Supplemental table SII

Abstract

The identification of proteins involved in brain ischemia might allow the discovery of putative biomarkers or therapeutic targets for ischemic stroke. Our aim is to study the distribution of proteins within mouse brain after an ischemic insult using MALDI Imaging-Mass-Spectrometry and to identify relevant proteins involved in brain damage. We occluded the middle cerebral artery of C57BL/6J mice. Brain slices were analyzed by MALDI-TOF and infarct (IC) and contralateral (CL) regions were compared using ClinProTools. The ion distribution maps of relevant m/z values were obtained by FlexImagin3.0. Protein identification was conducted through a bottom-up approach consisting on complementary sample fractionation methods. Some identifications were confirmed by immunohistochemistry and western blot. We identified 102 m/z values with different abundances between IC and CL ($p < 0.05$), from which 21 m/z peaks were selected as more relevant. Thirteen of them were found increased in the infarct region and 4 m/z values showed AUC > 90% between IC and CL. Identification analyses confirmed altered expressions of ATP5i, COX6C and UMP-CMP kinase in IC compared to CL.

Significance: Using MALDI-IMS we identified for the first time new proteins that might be involved in brain ischemia representing potential diagnostic biomarkers or target molecules for neurological recovery.

INTRODUCTION

Ischemic stroke is one of the most important neurological disorders and cause of disability worldwide[1]. Brain ischemia is originated by the impairment of blood supply into the brain parenchyma due to an arterial occlusion. This process encompasses a complex cascade of events that affects both cellular and extracellular matrix components including the inflammatory response, the immune cells extravasation, the development of edema or the blood-brain-barrier disruption[2]. Finally, it leads to cell death and tissue injury which is translated into a loss of neurological functions [3]. The identification of key molecules involved in brain injury and repair would help to design future treatments for neuroprotection and neurorecovery.

There are several experimental models of ischemic stroke developed in different species, especially rodents. The murine model which consists of the transient occlusion of the distal middle cerebral artery exhibits a reproducible cerebral infarct with a controlled reperfusion, low mortality rates and measurable neurological impairment during the acute phase[4,5]. This model is extremely useful for the study of cerebral ischemia pathophysiology and has been extensively used in the discovery of new molecules involved in brain injury [6–9].

MALDI imaging mass spectrometry (MALDI-IMS) is a powerful technique that allows to obtain the profiling of a broad range of molecules [10] such as metabolites[11–16], lipids[17–23], proteins[24–26] or drugs[27–31] directly on tissue[32]. In addition, it permits to analyze their spatial distribution and their local abundance simultaneously. This innovative technique has been proven to be useful for the molecular diagnostic in the context of inflammatory diseases[33–35], traumatic injuries[36,37], vascular diseases[17,38], neurodegenerative disorders[39] and specially in different types of tumors[40,41]. MALDI-IMS has been also employed for the study and visualization of lipid distribution in the brain after focal ischemia[42–44]. However, as far as we know a complete MALDI IMS profiling of proteins in the context of cerebral ischemia has not been yet conducted. The identification of new proteins involved in brain ischemia might allow the discovery of a new set of putative candidates to become biomarkers of

ischemic stroke and new potential therapeutic targets. This deeper knowledge would permit the study of pathways related with this severe disorder and its progression.

In our study we aim to visualize changes in the brain protein profile in a mouse model of brain ischemia and to identify new putative biomarkers or therapeutic targets by means of MALDI IMS.

METHODS

Animals

Adult male C57BL/6Ncr1 mice (body weight from 25 to 30 g) were used for the study. Animals were bred in-house in a temperature-/humidity- controlled room and maintained on a 12-hour light/ 12-hour dark cycle. The Ethics Committee of Animal Experimentation of Vall d'Hebron Research Institute approved the study protocol (No. 28/15), and all experiments were conducted in accordance with the Spanish legislation and the Directives of the European Union. The ARRIVE guidelines were considered when designing and reporting the results of the study. A total of 17 mice were included.

Transient middle cerebral artery occlusion (tMCAO)

The surgery was conducted as previously reported [5]. Briefly, mice were anesthetized with isoflurane (4% for induction, 2% for maintenance in air, 79% N₂ : 21% O₂; Abbot Laboratories, Madrid, Spain). Buprenorphin (0.05-0.1 mg/kg) was administered subcutaneously as analgesic for post-surgical pain. The distal part of the middle cerebral artery (MCA) was exposed after performing a small craniotomy in the left temporal bone, leaving the dura intact. The MCA was directly compressed for 60 min using a micromanipulator holding a 30G blunted needle decreasing the cerebral blood flow to <25% of the baseline values. After the arterial occlusion, the needle was removed and the cerebral blood flow (CBF) recovered at least the 75% of the baseline. During the entire procedure the body temperature was maintained at 36.5-37°C using a heating blanket and controlled by a rectal probe and the CBF was recorded by laser Doppler flowmetry (Moor Instruments, Devon, UK). After 24 hours animals were euthanized under deep anesthesia by cardiac perfusion as it follows: animals used for

MALDI-IMS profiling and other MS analyses for protein identification were perfused with cold saline, while those used for immunohistochemistry approaches were perfused with 4% cold paraformaldehyde (PFA).

MALDI IMS

Brain tissue processing, MALDI mass spectrometry and image analysis

Brains (n=4) were isolated and immediately snap frozen in isopentane (Sigma, USA) at -40°C during 30 sec and stored at -80°C. Ten μm -thick coronal brain sections (+0.74 to +0.98 from bregma) were obtained using a cryostat (Microm HM 505E, CBIS, USA) and mounted onto superconductive glass slides covered with ITO coating (Bruker Daltonics, Germany). Tissue preparations were dried with vacuum pump (Millipore, USA) at 600 mmHg for 15 minutes, washed for two minutes in 70% Ethanol and once in 96% Ethanol and then stored in a dessicator under vacuum. In order to be analyzed by MALDI TOF MS, samples were covered with sinapinic acid (10mg/mL in 60% acetonitrile and 0.2% trifluoroacetic acid (TFA)) as MALDI matrix sprayed using ImagePrep device (Bruker Daltonics). The device parameters were optimized for the brain sections, with a final set-up of 20 cycles combining 2,5s of spray, 5s of incubation and 20s of dry time. Finally the slides were mounted into MTP slide adapter (Bruker Daltonics) and transferred to the MALDI-TOF mass spectrometer. Four biologically independent samples were analyzed by MS. IMS spectra were acquired in linear positive ion mode in an UltrafleXtreme MALDI-TOF/TOF mass spectrometer (Bruker Daltonics). MS data were averaged from 300 consecutive laser shots with a frequency of 2,000 shot/s. The raster spatial resolution was 100 μm .

After the MS analysis, hematoxylin & eosin (H&E) staining (Sigma) was performed in each brain section and they were used as reference for colocalization to select the regions of interest (ROI).

Data quantification and statistical MALDI-IMS data analysis

After MALDI analysis, we used FlexImaging 3.0 (Bruker Daltonics, Germany) software to obtain ion density maps and to define the ROIs on each brain section. Two ROIs were defined on each brain section based on H&E staining. One ROI was defined on

the infarct core (IC) at the cerebral cortex and another ROI on the contralateral healthy (CL) area. In each brain section a dataset file was obtained with the spectra of each pixel contained in the ROIs. Then, all dataset files were combined in a single XML to be statistically analyzed with ClinProTools V3.0 software (Bruker Daltonics, Germany). The analysis of the mass spectra was focused on the mass range 2,000-24,000 m/z . The following settings were used for recalibration: a top hat baseline correction of 10% of minimal baseline width, a maximum peak shift of 2,000 ppm for peak alignment and 20% match to the calibrant peaks. Not recalibratable spectra were excluded from the statistical analysis. Signal to noise ratio for data acquisition was set to 5. An average spectrum from each ROI and the average peak list were obtained. Peak intensities were compared by t-test. In order to check the homogeneity of the spectra set we carried out principal components analysis (PCA) with the Matlab algorithm and used the 3 primary PCAs for the 3-D scaling representation. To select the most relevant m/z peaks from the average peak list we used the loading plot coupled to each PCA graphic. We also obtained the area under the curve (AUC) of each m/z peak to assess the discrimination between contralateral (CL) and infarct (IC) of each m/z peak.

Bottom-up protein identification strategies

We set up two parallel strategies in order to maximize the number of identified proteins with molecular masses matching our relevant m/z obtained from MALDI IMS analysis. A diagram of the followed experimental workflow is shown in figure 1.

Laser micro-dissection and protein extracts

We mounted consecutive brain cryosections of 12 μm thickness obtained from the same 4 brains analyzed by the MALDI-IMS. Brain sections were alternatively put on PEN-membrane slides (Leica, Germany) and superfrost glass slides (Thermo Scientific), and were finally stored at $-80\text{ }^{\circ}\text{C}$. Samples mounted on glass slides were used for IC localization through H&E staining and the same coordinates were used for laser microdissection. From the tissue sections mounted on PEN-membrane slides we dissected the IC and the CL areas (LMD6000 microscope, Leica) and recovered them separately into 25 μL of 0.1% Rapigest SF surfactant (Waters, USA). Samples were sonicated on ice at 80% amplitude for intervals of 10 sec for a total of 2 min. Then,

samples were centrifuged at 13,000g at 4°C, the supernatants were recovered, supplemented with 4.5 µL of aprotinin (Sigma) and 10 µL of phenylmethylsulfonyl fluoride (Sigma) as protease inhibitors, and finally stored at -80°C until use. The obtained homogenates were fractionated on a 10-20% Tris-tricine gel (Biorad, USA) under reducing condition and stained with colloidal coomassie G250 (Bio-Rad). Four sections of each sample, IC and CL area, were cut from the gel. The gel bands, corresponding to the proteins with an apparent molecular weight below 25 kDa, were digested in-gel with trypsin and subsequently analyzed by MS/MS.

Tissue homogenates and reverse phase HPLC (RP-HPLC)

For RP-HPLC separations, mechanical homogenates of IC and CL areas of mouse brain were obtained in 0.2% of TFA and 60% of acetonitrile (ACN). Samples were sonicated using the parameters described above. Insoluble material was removed by centrifugation at 13,000 g at 4°C, protease inhibitors were added into the recovered supernatant and samples were stored at -80°C until use. Soluble proteins were separated using the Alliance HPLC system (Waters) and a C4 widepore 3.6 µm; 4.6x100 mm Aeris reverse phase (RP) column (Phenomenex). Solvent A was 0.1% TFA in water and solvent B was 0.1% TFA in ACN. A linear gradient from 10 to 30% for 1 min, followed by a second step from 30 to 90% for 60 min was applied. Fractions were collected every 2 min, dried using a SpeedVac (Thermo Scientific) and reconstituted in 30 µL of H₂O 0.1 % TFA mixed at 1:1 volume ratio with sinapinic acid matrix (10 g/ml, in 1:2 H₂O:ACN, 0.2 % TFA). Finally samples were mounted onto a ground steel plate, let to crystalize and mass spectra were obtained by MALDI MS analysis (lineal mode, 24kV) to check for the presence of *m/z* of interest.

Bottom-up nano LC-MS/MS

Tryptic peptides from tricine gel sections and from RP-HPLC fractions of interest were analyzed on a LTQ Velos-Orbitrap mass spectrometer (ThermoFisher Scientific, Bremen, Germany) coupled to a nano-HPLC system (Proxeon Biosystems, Thermo Fisher Scientific, Bremen)). Briefly, peptide mixtures were initially concentrated on an EASY-column, 2 cm long, 100 µm internal diameter (id), and packed with ReproSil C18, 5 µm particle size (Proxeon, Thermo Fisher Scientific), and subsequently

chromatographed on an EASY-column, 75 μm id, 10 cm long, and packed with ReproSil-Pur C18-AQ, 3 μm particle size (Proxeon, Thermo Fisher Scientific). An ACN gradient (5– 35% ACN/0.1% formic acid in water, in 45 min, flow rate of 300 nL/min) was used to elute the peptides through a stainless steel nanobore emitter (Proxeon, Thermo Fisher Scientific) onto the nanospray ionization source of the LTQ Velos-Orbitrap mass spectrometer. MS/MS fragmentation spectra (200 ms, 100– 2800 m/z) of 20 of the most intense ions, as detected from a 500 ms MS survey scan (300–1500 m/z), were acquired using a dynamic exclusion time of 20 s for precursor selection and excluding single-charged ions. Precursor scans were acquired in the Orbitrap analyzer at a mass resolution of 30,000. MS/MS spectra were acquired at the LTQ Velos analyzer using normalized collision energy of 35%. An intensity threshold of 1,000 counts was set for precursor selection. Orbitrap measurements were performed enabling the lock mass option (m/z 445.120024) for survey scans to improve mass accuracy.

The mass spectrometry proteomics data have been deposited to the ProteomeXchange Consortium[45] via the PRIDE partner repository with the dataset identifier PXD003644 and 10.6019/PXD003644.

Bioinformatics for protein identification

LC-MS/MS data were analyzed using the Proteome Discoverer software (Thermo Fisher Scientific) to generate mgf files. Processed runs were loaded to ProteinScape software (Bruker Daltonics, Bremen, Germany) and peptides were identified using Mascot (Matrix Science, London UK) to search the SwissProt 20160108 database, restricting taxonomy to *mus musculus* (16754 sequences). MS/MS spectra were searched with a precursor mass tolerance of 10 ppm, fragment tolerance of 0.05 Da, trypsin specificity with a maximum of 2 missed cleavages, cysteine carbamidomethylation set as fixed modification and methionine oxidation as variable modification. Significance threshold for the identifications was set to minimum ions score of 20, and the identification results were filtered to 1% FDR at peptide level, based on searches against a Decoy database

In order to match the relevant identified m/z peaks after MALDI IMS with the molecular masses of the proteins identified by bottom-up analysis, we used the PeptideMass tool from ExPasy (http://web.expasy.org/peptide_mass/)[46]. This tool allows the generation of the theoretical peptide masses of the input proteins. By selecting the “no cutting” parameter, all the putative fragments resulting after the post-translational processing of each protein were displayed (i.e. pro-form, signal sequences, transit peptides, active peptide, etc). All known post-translational modifications (PTMs) and variants of the proteins were considered and all other parameters were used as default. The identified MALDI-IMS m/z peaks were matched with the masses of proteins and/or peptides retrieved by PeptideMass considering a maximum mass shift of 2,000 ppm, which corresponds to the maximum peak shift allowed in peak alignment during the recalibration of MALDI IMS spectra.

Verification of candidates

Immunohistochemistry

Some of the predicted proteins were selected based on their biological function and the availability of commercial antibodies to be confirmed by immunohistochemistry. Sections of 12 μm of thickness (+0.5 to +1.9 μm from bregma) were obtained from mouse brains previously fixed with PFA. The brains were cryoprotected with 30% sucrose in PBS, embedded in OCT and kept at -80°C until use (N=4-5). Brain sections were acetone-fixed and subjected to antigen retrieval in citric acid (pH=6 / 95°C). Endogenous peroxidases were inactivated using 2% H_2O_2 and tissue was blocked with goat serum (5% in PBS- 0.1% tween) for 1 hour. Finally tissue sections were incubated overnight at 4°C with the corresponding primary anti-mouse antibody produced in rabbit against ATP5i (1/50) (Proteintech, USA), UMP-CMP Kinase (1/50) (Proteintech), COX6C (1/100) (Biorbyt, UK), FXYD7 (1/100) (Biorbyt), PLM (1/100) (Biorbyt), Nedd8 (1/80)(Enzolifesciences, USA), ubiquitin (1/250) (Novus, USA), NEUG (1/500) (Proteintech), PDCD5 (1/25) (Proteintech). Biotinilated IgG anti-rabbit was applied as secondary antibody (Vector Laboratories, Burlingame, USA). Detection was performed using DAB systems (Dako, Denmark) followed by hematoxylin (Sigma) counterstaining. Negative controls were included in each case without the corresponding primary

antibody. For immunohistochemistry quantification images were acquired (200x) from the IC region and from the CL equivalent section (2 images per region corresponding to the primary somatosensory area layer 2/3 and layer 5). Images from the respective negative control were used to set the threshold to consider positive staining when primary antibodies were present. Positive area was quantified using standard computer assisted technique based on ImageJ FIJI software. The IC positive-stained areas were normalized considering the corresponding CL quantified areas. Statistical comparisons were performed using T-test (SPSS 15.0 software). Mean and standard error are represented and a p-value less than 0.05 was considered significant for all comparisons.

Western blot

Mouse brain homogenates (n=3) of CL and IC areas were obtained and resolved on 10-20% Tris-tricine gel under reducing conditions and transferred onto 0.45m polyvinylidene difluoride membranes (Millipore Corp). Membranes were blocked for 1 hour with 10% nonfat milk (PBS 0.1% Tween 20) and later probed with anti-ATP5i (1/1000), anti- COX6C (1/800), anti- UMP-CMP Kinase (1/1000) and anti- β actin (1/20000) overnight at 4°C. Secondary antibodies (Chemicon International) anti-rabbit-horseradish peroxidase (1:1000) from donkey or anti-mouse-horseradish peroxidase (1:1000) from sheep, were used for 1h incubations at room temperature with gentle agitation. Three washes with PBS-Tween were performed before and after the incubation with secondary antibodies. The substrate reaction was developed with chemiluminescent reagent Luminol (Amersham Biosciences, UK) and analyzed with LAS-3000 luminescent analyzer (Fujifilm, USA). Scanned Western blots were quantified using Image-J free software. Positive signal was corrected by actin used as loading control. IC-positive bands were normalized by the CL quantified bands and statistical comparisons were performed using T-test (SPSS 15.0 software). Mean and standard error are represented and a p-value less than 0.05 was considered significant for all comparisons.

Results

MALDI IMS

We obtained the average spectra of the infarct (IC) and the contralateral (CL) healthy areas, and identified a total of 102 m/z values with different intensities between both regions ($p < 0.0001$) (Figure 2A). PCA analysis revealed a good discrimination between IC and CL when PC1 was combined with PC2 and PC3 (Figure 2B). Using loading plot analysis we selected the 21 most-relevant m/z values (Figure 2B and 2C) and subsequently obtained their ion distribution map to visualize their positioning along the whole brain sections. All the m/z peaks colocalized with the injured infarcted area revealing an increase or a decrease in its relative abundance (table 1).

Four out of the 21 most relevant m/z peaks showed a very high discrimination capacity between IC and CL with $AUC > 0.9$ (figure 3). When other parts of the brain sections were visualized, the peak m/z 6726 was found more abundant in the ventral striatum whereas the peaks m/z 7545 and m/z 4815 were found increased in the cerebral cortex and the region of the pallidum respectively. In contrast, m/z 8458 appeared significantly increased in the IC area when compared with the equivalent region in the CL area and only the anterior commissure retrieved an elevated abundance compared to other parts of the healthy tissue. (Figure 3).

Protein identification by Bottom-up approach

We obtained the protein extract of the IC and CL areas from adjacent brain sections by means of laser microdissection and fractionated them through 1D tricine gels. Given that the proteins that were found most relevant in terms of discrimination capacity after MALDI-IMS analysis ranged from 4,285 to 22,178 m/z , the regions of the tricine gels comprised between 4 and 23 KDa were cut and digested with trypsin. After nanoLC-MS/MS analysis we identified a total of 666 proteins with at least 2 unique peptides: 257 were only found in CL, 61 in IC and 348 proteins were identified in homogenates from both regions, CL and IC (Supplemental table S1). After determining the masses of the identified proteins considering all the described PTMs, we matched 8 m/z peaks with the MALDI-IMS results (Table 2).

In a parallel approach we fractionated IC and CL brain homogenates by RP-HPLC using a C4 column and analyzed the obtained fractions by MALDI MS. The chromatographic peaks with corresponding retention times of 24, 26 and 28 minutes contained m/z

values similar to some of the relevant m/z detected by MALDI-IMS (5708.072, 8110.952, 8108.42, 8569.93, 8567.025, 6721.464, 7533.73, 22176.646)(Figure 4). These fractions were digested using trypsin and then analyzed through nanoLC-MS/MS. As a result a total of 495 proteins were identified with ≥ 2 unique peptides (Supplemental table S2). Among the identified proteins we found matches for the m/z 5708.072, 8110.95, 8569.93 and 8569.9, all of them previously reported in the MALDI-IMS experiment. The proteins corresponding to these m/z were ATP5e, ATP5i, Nedd8 and ubiquitin, which were identified with a sequence coverage $>35\%$ and an identification SCORE >60 (Table 3).

Immunohistochemistry

After the immunohistochemistry analysis, the proteins ATP5i and COX6C showed a higher expression in the IC region compared to the CL area ($p < 0.05$ and $p < 0.2$, respectively). In contrast, UMP-CMP kinase showed a significant decrease ($p < 0.01$), confirming the results obtained by MALDI-IMS (Figure 5A, 5B and 5C).

Western Blot

As expected, western blot analyses in IC and CL regions from brain homogenates showed that, ATP5i expression was increased in IC whereas UMP-CMPK was decreased. In contrast, no differences were found in COX6C expression when both regions were compared.

Discussion

The present study shows for the first time the profiling and spatial distribution of proteins along different regions of mouse brain subjected to focal ischemia using the state of the art technique MALDI IMS.

During the last decade, the identification of the protein identity related to each m/z peak has generally been elusive in studies applying MALDI-IMS, precluding the validation of the results and the elucidation of the biological processes involved. However, different identification approaches have been developed by MALDI imaging users. Indirect identifications correlating proteomic strategies (i. e. bottom-up) and

imaging data represent an effective approach for protein identity verification [47]. An alternative strategy that has been proven successful consist of the comparison of the presence and distribution of the protein of interest between wild type animals and knockout experimental models [48,49]. Recently, important steps forward were made with the optimization of on-tissue digestion protocols [50]. Following tryptic digestion, protein identification can be reached after the analysis of the generated peptides. However, low fragmentation efficiencies and high background signal are important challenges to overcome. A significant advancement was achieved in molecular imaging strategies with the use of MALDI FITCR IMS for the analysis of tissue sections [51,52]. MALDI FITCR IMS provides the highest mass resolution and accuracy and allows the obtaining of high spatial resolution images. These improvements might facilitate a substantial progress to effectively link proteomic experiments with imaging data in future studies thanks to the application of next generation analytical tools.

In our study, after MALDI IMS analysis, we followed a bottom-up strategy to correlate imaging with proteomic analyses. As a result we identified a total of 21 relevant protein species differently expressed in IC compared to the CL region. We were able to identify different proteins after the development and combination of different sample fractionation methods based on size or hydrophobicity separation. In addition, after the bottom-up analysis we took into account the putative post-translationally modified forms of the identified proteins to become one step closer to the real tissue phenotype, where PTMs and protein processing occur. Following this strategy we identified and confirmed ATP5i, COX6C and UMP-CMP kinase as proteins related to brain ischemia.

During cerebral ischemia the production of cellular energy is impaired and ATP concentration decreases promoting the depolarization of the neuron membranes and causing an imbalance of Na^+ , K^+ and Ca^{2+} [53]. This alteration of the ion homeostasis induces the release of neurotransmitters, further inhibits the production of ATP and activates endogenous proteases enlarging the cytotoxic response to ischemia. Ischemic injury also increases the amounts of reactive oxygen species (ROS) which attack key cellular components, especially in the reperfused regions [54]. We identified two proteins, ATP5i and COX6C, which are increased in the ischemic tissue when compared

with the healthy contralateral area of the brain. Both proteins are members of the oxidative phosphorylation pathway (OXPHOS) thus involved in the production of energy in eukaryotic cells resulting from the oxidation of nutrients. ATP5i is the subunit e of the F₀ complex, which comprises the proton channel in the ATP synthase complex in the inner membrane of the mitochondria [55]. Our results are in line with others' in which ATP synthase complex 5 together with other mitochondrial proteins has been found increased in the middle cerebral arteries isolated from the ischemic region compared with the healthy area and non-ischemic animals [56]. After MALDI IMS analysis we also found the *m/z* 5712 increased in IC. This *m/z* value might correspond to the ATP synthase complex subunit ATP5E although these results could not be replicated by immunohistochemistry. In contrast, ATP5 subunit beta has been found significantly decreased in rat cortical neurons after chemically induced ischemia [57]. These divergences might reflect the different response to ischemia of the components of the neurovascular unit. Similarly to ATP5i, we found an increased abundance of the Cytochrome c oxidase (COX) complex subunit COX6C in the IC of the brain compared to the CL area. COX6C is a nuclear-coded polypeptide that is tightly bound to the catalytic subunits I and II [58] and its expression together with other COX subunits has been found altered in neurological diseases such as Alzheimer's [59]. Although no specific function has been yet described for COX6C it may be involved in the regulation and assembly of the complex COX. COX is the last heteromeric complex (complex IV) of the mitochondrial respiratory chain that catalyzes the electron transfer to oxygen. Its inhibition due to the lack of oxygen is a central initial process of the ischemic damage [60]. The increase of ATP5i and COX6C expression found through our analysis by MALDI-IMS might be promoted by the requirement of a greater mitochondrial function to restore oxidative phosphorylation after ischemia. This compensatory effect against the lack of oxygen might be promoted by the increase of total mitochondrial mass after ischemia due to mitochondrial biogenesis [61,62]. Interestingly, COX activity has been found altered after ischemic stroke in cerebrospinal fluid and erythrocyte hemolysate of patients compared to healthy controls [63]. In other analyses performed in brain tissue, some authors have found increased expression of COX subunit I after global cerebral ischemia [64]. In contrast, others have found a COX subunit I decrease in the region of the infarct core after a tMCAo of 90 min and 48h of reperfusion [65].

These controversies may reflect the dependence of the process on the time of ischemia and reperfusion [66]. Deficiencies in COX function, expression or assembly have been related with other diseases such as the mitochondrial disorders Leigh Syndrome [67], neonatal hypertrophic cardiomyopathy [68] or early-onset leukodystrophic encephalopathy [69].

The modulation of proteins members of the OXPHOS pathway has been already considered for neuroprotection [70,71]. Although the strategies of ROS scavenging have resulted futile, the uncoupling of mitochondrial membrane potential through the stimulation of proton channels and the induction of OXPHOS complexes phosphorylation seem promising approaches that may reduce the effects of ischemia [66]. Our results suggest the implication of the subunits ATP5i and COX6C in the brain infarct development, thus presenting them as potential molecules to modulate and minimize neuronal injury.

On the other hand, UMP-CMP kinase acts as an uridylylate-cytidylylate kinase that catalyzes the phosphorylation of CMP and UMP with the consequent formation of the nucleosides CDP and UDP, which are further phosphorylated to its triphosphate forms at the expense of ATP [72]. These nucleosides are required for the cellular nucleic acid synthesis [73] but they also play important roles in neuronal function. More precisely, they are involved in the regulation of adenylate cyclase and protein synthesis, as well as sugar metabolism, synthesis of phospholipids and release of neurotransmitter [74]. During brain ischemia, a decrease in the levels of CTP and UTP has been observed [75], and the exogenous administration of these nucleosides has been proven to be neuroprotective in different models of brain ischemia [74]. A decreased expression of UMP-CMP kinase in the mouse cerebral cortex has been related to aging [76] but, to our knowledge, no study has explored UMP-CMP kinase in brain ischemia. In this regard we found a decreased expression of UMP-CMP kinase in the IC compared to the CL healthy area of mouse brain. This finding suggests that UMP-CMP kinase might play a role in the modulation and promotion of the pyrimidine nucleoside metabolism restoration after ischemia, which could be accompanied by a recovery of the brain function.

The application of MALDI-imaging allowed us to compare the relative abundance of proteins at different regions of interest and to identify new potential biomarkers of brain ischemia or candidate therapeutic targets for tissue recovery. After the combination of two different identification strategies after bottom-up analysis, four proteins were identified in both approaches.

Our study stands with some limitations. Despite different attempts, we were not able to obtain good quality spectra after on-tissue trypsin digestion (data not shown). The results of this analysis might have permitted the identification of further putative candidates. By the development of the strategies presented in our study we were able to identify different protein candidates, however, apart from COX6C (m/z 8458), we failed to identify other m/z that retrieved a very high discrimination ability between IC and CL (with $AUC > 0.9$). In addition, we were not able to obtain chromatographic fractions highly enriched with proteins of interest in order to perform a top-down approach for protein identification (not shown). The protein identification based on bottom-up analysis is limited by i) the mass error inherent to MALDI-imaging in the analysis of intact proteins, and ii) the presence of PTMs which can difficult the protein mass calculation based on the aminoacid sequence. The mass tolerance considered to link the MALDI IMS data with bottom-up results was 2,000 ppm, a narrow tolerance window similar to other authors' [36,77,78]. During this process, all PTMs that are described for each protein were taken into account although protein- m/z matching based on molecular weight is complex especially in the analysis of big biomolecules. Thus, the presence of false negative and false positive identifications cannot be excluded. In spite of that, we validated some of the candidates by orthogonal methodologies and found patterns of expression which are coherent with MALDI imaging data. Our identification strategy might be improved in near future considering unspecific protein degradation by endogenous proteases.

Future additional studies are needed to confirm our findings. The application of MALDI IMS in other models of brain ischemia and with different times of occlusion might also help in finding proteins involved in the early response to brain ischemia. Future studies will assess the value of the identified proteins as biomarkers in human stroke.

Conclusion

We characterized for the first time the protein profile and distribution of brain subjected to ischemia and we were able to determine changes in protein abundance in a murine model using MALDI imaging MS. Proteomic results were confirmed by immunohistochemistry and western blot in independent samples and the identified candidates might represent putative candidates to become biomarkers or molecular targets in brain ischemia.

Funding sources

Neurovascular Research Laboratory takes part into the Spanish stroke research network INVICTUS (RD12/0014/0005) and is partially funded by grants from the Fondo de Investigaciones Sanitarias (PI11/00176), Instituto de Salud Carlos III. VHIO Proteomics Laboratory is a member of Proteored, PRB2-ISCIII and is supported by grant PT13/0001, of the PE I+D+i 2013-2016, funded by Instituto de Salud Carlos III. M. Hernández-Guillamon is supported by the Miquel Servet programme (CP12/0359) and A. Rosell is supported by the Miguel Servet program (CPII15/00003), both from the Instituto de Salud Carlos III. A. Simats holds a predoctoral fellowship (2015 FI_B 00952) from the AGAUR. F. Ma is supported by a predoctoral Fellowship from the China Scholarship Council. Several of these research programs are co-financed by the European Regional Development Fund (ERDF). SA Trejo is member of the CONICET Researcher Career.

Notes

All authors declare no conflict of interest.

FIGURES

Figure 1: Diagram of the experimental workflow followed for the analysis of mouse brain after ischemia by MALDI-IMS. Two parallel strategies with different sample fractionation approaches were performed. In a first approach, protein extracts from infarct core (IC) and healthy contralateral area (CL) were obtained by means of laser micro-dissection and were separated using a tricine gel. In a second approach, tissue homogenates from both IC and CL were fractionated by RP-HPLC and fractions were analyzed by MALDI MS. Both, the bands excised from tricine gels, and the fractions of interest obtained from RP-HPLC, were trypsin digested and analyzed using an Orbitrap LTQ velos mass spectrometer.

Figure 2: A) Average spectra obtained from the regions of interest (ROIs) considered for the comparative analysis. ROI 1 corresponds to the infarct core (IC) on the cortical region, whereas ROI 2 was set on the corresponding healthy contralateral (CL) area of the brain (n=4). B) Principal Components Analysis (PCA) of the obtained spectra showed the discrimination of both ROIs based on the obtained mass spectra. Each dot from the dot plot represent a mass spectra obtained from IC (red) and CL (green). C) The 102 m/z peaks that showed significant differences between IC and CL are distributed in loading plots. Some of the 21 most relevant m/z peaks appear highlighted. I: m/z 8458; II: m/z 8573; III: m/z 6855; IV: m/z 4815; V: m/z 6726; VI: m/z 5449; VII: m/z 7545; VIII: m/z 6655; IX: m/z 4969; X: m/z 14999; XI: m/z 15630. Scale bar, 500 μ m.

Figure 3: Ion density maps corresponding to m/z 6726, m/z 7545, m/z 4815 and m/z 8458. Peaks 6726, 7545 and 4815 show a reduced intensity in the infarct region when compared with the healthy contralateral area. Red-white pixels represent a high abundance whereas blue-dark pixels correspond to regions with low abundance or absence of the corresponding m/z . The image on the right represents the hematoxylin&eosin staining of the corresponding brain section after being analyzed by MALDI-IMS. Area under the curve (AUC) are indicated for each m/z value. Scale bar, 500 μ m.

Figure 4: Mass spectra obtained after the analysis by MALDI MS of the fractions obtained by reverse phase HPLC. The corresponding retention times were 24 (A), 26 (B) and 28 (C) min, respectively. The arrows indicate those m/z that had been identified by MALDI-IMS as putative discriminatory peaks. These fractions were digested with trypsin and analyzed through nanoLC MS/MS. The identified proteins were matched with the corresponding MALDI MS m/z , taking into account their molecular weight (m. w.) including post-translational modifications. The m/z 8108.426 matched with ATP5i (m. w. of 8100.43, after loss of initial methionine); the m/z 8569.934 and m/z 8567.025 matched with ubiquitin (m. w 8560.62 Da) and Nedd8 (m. w. 8555.67 Da, after loss of C-terminal fragment); and the m/z 5708.072 matched with ATP5E (m. w. of 704.12 Da, after loss of initial methionine).

Figure 5: Identification of ATP5i (corresponding to m/z 8112)(A), COX6C ($m/z=8458$)(B) and UMP-CMP kinase ($m/z=22178$)(C) were confirmed by IHC. The percentage of positive signal was determined in 2 fields from each region of interest and averaged. The percentage of positive signal is represented as normalized signal considering CL as reference. (D) Western blot analysis of ATP5i, COX6C and UMP-CMP kinase in mouse brain homogenates.

* $p<0.05$, ** $p<0.01$; # $p<0.2$

Scale bar in immunohistochemistry images: 50 μm (200X)

Scale bar in MALDI imaging and H&E staining: 500 μm

ATP5i: ATP synthase subunit e; COX6C: cytochrome oxidase subunit VI C; CL: contralateral; IC: infarct core.

Table 1: Most relevant 21 *m/z* peaks identified after MALDI-IMS analysis.

<i>m/z</i> peak	CL vs IC	CL average intensity (a. u.)	IC average intensity (a. u.)
4286	CL<IC	3.75±0.27	5.68±0.55
4752	CL>IC	6.73±0.60	3.59±0.79
4815	CL>IC	14.03±1.96	3.54±0.56
4942	CL>IC	11.09±2.60	6.39±0.77
4969	CL>IC	48.01±3.74	16.95±2.44
5175	CL>IC	6.04±0.43	4.18±0.60
5712	CL<IC	5.16±0.54	7.17±0.86
6282	CL>IC	7.78±2.03	4.04±0.66
6655	CL>IC	9.81±3.19	4.33±0.47
6726	CL>IC	37.99±10.84	8.43±2.13
7074	CL>IC	8.26±1.02	4.67±0.63
7545	CL>IC	24.41±7.75	4.62±0.35
8112	CL<IC	3.69±0.25	4.38±0.60
8458	CL<IC	2.86±0.14	6.27±0.63
8499	CL<IC	3.30±0.16	4.51±0.36
8573	CL<IC	15.48±3.08	24.33±3.10
8738	CL<IC	2.50±0.23	4.06±0.57
9088	CL>IC	5.58±0.22	3.24±0.60
14145	CL>IC	13.28±2.83	3.73±1.02
14999	CL<IC	1.08±0.08	1.77±0.62
22178	CL>IC	1.76±0.30	1.14±0.25

All *m/z* showed a p-value <0.000001

a.u.: arbitrary units; CL: contralateral; IC: infarct core; p-value: p-value after t-student-ANOVA comparison between peak intensities

Table 2: Matching between the *m/z* peaks from MALDI-IMS and the proteins identified after SDS-tricine gels followed by nanoLC-MS/MS analysis.

MALDI imaging <i>m/z</i>	Swissprot accession code	Protein name	Id SCORE (CL, IC)	SC% (CL, IC)	Predicted PTM	MW (Da)
6282	USMG5_MOUSE	Up-regulated during skeletal muscle growth protein 5	80.4, 47	44.8, 17.2	loss of initial methionine + 1 acetylation	6289
22178	RAB1B_MOUSE	Ras-related protein Rab-1B	281.3, 36.5	34.3, 7.5	-	22174.23
	KCY_MOUSE	UMP-CMP kinase	35.6, 55.2	11.2, 12.8	1 acetylation	22194.34
14145	PDCD5_MOUSE	Programmed cell death protein 5	129, --	30.2, -	loss of initial methionine	14136.31
	NDUC2_MOUSE	NADH dehydrogenase [ubiquinone] 1 subunit C2	71.2, 41.8	10.8, 16.7	-	14155.24
8458	COX6C_MOUSE	Cytochrome c oxidase subunit 6C	356.3, 184.5	72.4, 56.6	-	8464.51
5712	ATP5E_MOUSE	ATP synthase subunit epsilon, mitochondrial	93.9, 73.2	53.8, 73.1	loss of initial methionine	5704.12
8499	FXYP7_MOUSE	FXYP domain-containing ion transport regulator 7	99.7, 70.4	20, 20	-	8482.25
	PLM_MOUSE	Phospholemman	57.3, 50.6	21.7, 21.7	loss of signal peptide and 2 phosphorylations	8508.34
7545	NEUG_MOUSE	Neurogranin	144.3, 102.6	26.9, 26.9	1 acetylation	7534
8573	NEDD8_MOUSE	NEDD8	89.1, -	38.3, -	loss of c-terminal	8555.67
	RS27A_MOUSE	Ubiquitin-40S ribosomal protein S27a	938.1, 486.5	32.7, 25	Chain Ubiquitin at positions 1 - 76	8560.62
8112	ATP5I_MOUSE	ATP synthase subunit e, mitochondrial	360.7, 73.6	57.7, 39.4	loss of initial methionine	8100.43

Id SCORE: score of identification; SC%: percentage of sequence coverage; PTM: post-translational modifications; MW: molecular weight considering the corresponding PTM.

Table 3: Correspondence between the *m/z* peaks from MALDI-IMS and the proteins identified after RP-HPLC fractionation of brain homogenates and nanoLC-MS/MS analysis.

MALDI IMS <i>m/z</i>	MALDI <i>m/z</i>	Swissprot accession code	Protein name	Id SCORE	SC%	Predicted PTM	MW (Da)	Fraction RT (min)
8112	8110.95	ATP5I_MOUSE	ATP synthase subunit e, mitochondrial	6199	71.8	loss of initial methionine	8100.43	24, 26
8573	8569.93	RS27A_MOUSE	Ubiquitin-40S ribosomal protein S27a	1507.3	28.2	Ubiquitin fragment	8560.62	24, 26, 28
8573	8569.93	NEDD8_MOUSE	NEDD8	221.6	51.9	loss of c-terminal fragment	8555.67	24, 26
						Ubiquitin fragment	8560.62	24, 26
5712	5708.07	ATP5E_MOUSE	ATP synthase subunit epsilon	64.8	44.2	loss of initial methionine	5704.12	24, 26

Id SCORE: score of identification; SC%: percentage of sequence coverage; PTM: post-translational modifications; MW: molecular weight considering the corresponding PTM. RT: retention time in RP-HPLC

References

- [1] D. Mozaffarian, E.J. Benjamin, A.S. Go, D.K. Arnett, M.J. Blaha, M. Cushman, S. de Ferranti, J.-P. Després, H.J. Fullerton, V.J. Howard, M.D. Huffman, S.E. Judd, B.M. Kissela, D.T. Lackland, J.H. Lichtman, L.D. Lisabeth, S. Liu, R.H. Mackey, D.B. Matchar, D.K. McGuire, E.R. Mohler, C.S. Moy, P. Muntner, M.E. Mussolino, K. Nasir, R.W. Neumar, G. Nichol, L. Palaniappan, D.K. Pandey, M.J. Reeves, C.J. Rodriguez, P.D. Sorlie, J. Stein, A. Towfighi, T.N. Turan, S.S. Virani, J.Z. Willey, D. Woo, R.W. Yeh, M.B. Turner, American Heart Association Statistics Committee and Stroke Statistics Subcommittee, Heart disease and stroke statistics--2015 update: a report from the American Heart Association, *Circulation*. 131 (2015) e29-322. doi:10.1161/CIR.000000000000152.
- [2] S.E. Lakhan, A. Kirchgessner, M. Hofer, Inflammatory mechanisms in ischemic stroke: therapeutic approaches, *J. Transl. Med.* 7 (2009) 97. doi:10.1186/1479-5876-7-97.
- [3] F. López-Neblina, Alexander H. Toledo, Molecular Biology of Apoptosis in Ischemia and Reperfusion - Journal of Investigative Surgery - Volume 18, Issue 6, *J. Invest. Surg.* 18 (2005) 335–350.
- [4] I.M. Macrae, Preclinical stroke research--advantages and disadvantages of the most common rodent models of focal ischaemia, *Br. J. Pharmacol.* 164 (2011) 1062–1078. doi:10.1111/j.1476-5381.2011.01398.x.
- [5] A. Morancho, L. García-Bonilla, V. Barceló, D. Giralt, M. Campos-Martorell, S. Garcia, J. Montaner, A. Rosell, A new method for focal transient cerebral ischaemia by distal compression of the middle cerebral artery: Transient dMCAO by artery compression, *Neuropathol. Appl. Neurobiol.* 38 (2012) 617–627. doi:10.1111/j.1365-2990.2012.01252.x.
- [6] D. Brea, J. Agulla, A. Staes, K. Gevaert, F. Campos, T. Sobrino, M. Blanco, A. Dávalos, J. Castillo, P. Ramos-Cabrer, Study of Protein Expression in Peri-Infarct Tissue after Cerebral Ischemia, *Sci. Rep.* 5 (2015) 12030. doi:10.1038/srep12030.
- [7] K. Suzuyama, T. Shiraishi, T. Oishi, S. Ueda, H. Okamoto, M. Furuta, T. Mineta, K. Tabuchi, Combined proteomic approach with SELDI-TOF-MS and peptide mass fingerprinting identified the rapid increase of monomeric transthyretin in rat cerebrospinal fluid after transient focal cerebral ischemia, *Brain Res. Mol. Brain Res.* 129 (2004) 44–53. doi:10.1016/j.molbrainres.2004.06.021.
- [8] X. Xiong, Q. Liang, J. Chen, R. Fan, T. Cheng, Proteomics profiling of pituitary, adrenal gland, and splenic lymphocytes in rats with middle cerebral artery occlusion, *Biosci. Biotechnol. Biochem.* 73 (2009) 657–664. doi:10.1271/bbb.80717.
- [9] C. Ren, J. Guingab-Cagmat, F. Kobeissy, S. Zoltewicz, S. Mondello, M. Gao, A. Hafeez, N. Li, X. Geng, S.F. Larner, J. Anagli, R.L. Hayes, X. Ji, Y. Ding, A neuroproteomic and systems biology analysis of rat brain post intracerebral hemorrhagic stroke, *Brain Res. Bull.* 102 (2014) 46–56. doi:10.1016/j.brainresbull.2014.02.005.
- [10] M. Aichler, A. Walch, MALDI Imaging mass spectrometry: current frontiers and perspectives in pathology research and practice, *Lab. Investig. J. Tech. Methods Pathol.* 95 (2015) 422–431. doi:10.1038/labinvest.2014.156.
- [11] J. Wang, S. Qiu, S. Chen, C. Xiong, H. Liu, J. Wang, N. Zhang, J. Hou, Q. He, Z. Nie, MALDI-TOF MS imaging of metabolites with a N-(1-naphthyl) ethylenediamine dihydrochloride matrix and its application to colorectal cancer liver metastasis, *Anal. Chem.* 87 (2015) 422–430. doi:10.1021/ac504294s.
- [12] D.R. Bhandari, M. Schott, A. Römpf, A. Vilcinskas, B. Spengler, Metabolite localization by atmospheric pressure high-resolution scanning microprobe matrix-assisted laser desorption/ionization mass spectrometry imaging in whole-body sections and individual organs of the rove beetle *Paederus riparius*, *Anal. Bioanal. Chem.* 407 (2015) 2189–2201. doi:10.1007/s00216-014-8327-1.

- [13] D.R. Bhandari, Q. Wang, W. Friedt, B. Spengler, S. Gottwald, A. Römpf, High resolution mass spectrometry imaging of plant tissues: towards a plant metabolite atlas, *The Analyst*. 140 (2015) 7696–7709. doi:10.1039/c5an01065a.
- [14] D. Miura, Y. Fujimura, H. Wariishi, In situ metabolomic mass spectrometry imaging: recent advances and difficulties, *J. Proteomics*. 75 (2012) 5052–5060. doi:10.1016/j.jprot.2012.02.011.
- [15] A. Ly, A. Buck, B. Balluff, N. Sun, K. Gorzolka, A. Feuchtinger, K.-P. Janssen, P.J.K. Kuppen, C.J.H. van de Velde, G. Weirich, F. Erlmeier, R. Langer, M. Aubele, H. Zitzelsberger, L. McDonnell, M. Aichler, A. Walch, High-mass-resolution MALDI mass spectrometry imaging of metabolites from formalin-fixed paraffin-embedded tissue, *Nat. Protoc.* 11 (2016) 1428–1443. doi:10.1038/nprot.2016.081.
- [16] D. Sturtevant, Y.-J. Lee, K.D. Chapman, Matrix assisted laser desorption/ionization-mass spectrometry imaging (MALDI-MSI) for direct visualization of plant metabolites in situ, *Curr. Opin. Biotechnol.* 37 (2016) 53–60. doi:10.1016/j.copbio.2015.10.004.
- [17] M. Martin-Lorenzo, B. Balluff, A.S. Maroto, R.J. Carreira, R.J.M. van Zeijl, L. Gonzalez-Calero, F. de la Cuesta, M.G. Barderas, L.F. Lopez-Almodovar, L.R. Padial, L.A. McDonnell, F. Vivanco, G. Alvarez-Llamas, Lipid and protein maps defining arterial layers in atherosclerotic aorta, *Data Brief*. 4 (2015) 328–331. doi:10.1016/j.dib.2015.06.005.
- [18] E.B. Yalcin, S.M. de la Monte, Review of matrix-assisted laser desorption ionization-imaging mass spectrometry for lipid biochemical histopathology, *J. Histochem. Cytochem. Off. J. Histochem. Soc.* 63 (2015) 762–771. doi:10.1369/0022155415596202.
- [19] D. Gode, D.A. Volmer, Lipid imaging by mass spectrometry – a review, *Analyst*. 138 (2013) 1289–1315. doi:10.1039/C2AN36337B.
- [20] H. Tanaka, N. Zaima, T. Sasaki, N. Yamamoto, K. Inuzuka, M. Sano, T. Saito, T. Hayasaka, N. Goto-Inoue, K. Sato, H. Kugo, T. Moriyama, H. Konno, M. Setou, N. Unno, Imaging Mass Spectrometry Reveals a Unique Distribution of Triglycerides in the Abdominal Aortic Aneurysmal Wall, *J. Vasc. Res.* 52 (2015) 127–135. doi:10.1159/000439169.
- [21] E.E. Jones, S. Dworski, D. Canals, J. Casas, G. Fabrias, D. Schoenling, T. Levade, C. Denlinger, Y.A. Hannun, J.A. Medin, R.R. Drake, On-tissue localization of ceramides and other sphingolipids by MALDI mass spectrometry imaging, *Anal. Chem.* 86 (2014) 8303–8311. doi:10.1021/ac501937d.
- [22] J.A. Hankin, S.E. Farias, R.M. Barkley, K. Heidenreich, L.C. Frey, K. Hamazaki, H.-Y. Kim, R.C. Murphy, MALDI mass spectrometric imaging of lipids in rat brain injury models, *J. Am. Soc. Mass Spectrom.* 22 (2011) 1014–1021. doi:10.1007/s13361-011-0122-z.
- [23] P.M. Angel, J.M. Spraggins, H.S. Baldwin, R. Caprioli, Enhanced sensitivity for high spatial resolution lipid analysis by negative ion mode matrix assisted laser desorption ionization imaging mass spectrometry, *Anal. Chem.* 84 (2012) 1557–1564. doi:10.1021/ac202383m.
- [24] C.H. Na, J.H. Hong, W.S. Kim, S.R. Shanta, J.Y. Bang, D. Park, H.K. Kim, K.P. Kim, Identification of Protein Markers Specific for Papillary Renal Cell Carcinoma Using Imaging Mass Spectrometry, *Mol. Cells*. 38 (2015) 624–629. doi:10.14348/molcells.2015.0013.
- [25] R. Casadonte, M. Kriegsmann, S.-O. Deininger, K. Amann, R. Paape, E. Belau, D. Suckau, J. Fuchser, J. Beckmann, M. Becker, J. Kriegsmann, Imaging mass spectrometry analysis of renal amyloidosis biopsies reveals protein co-localization with amyloid deposits, *Anal. Bioanal. Chem.* 407 (2015) 5323–5331. doi:10.1007/s00216-015-8689-z.
- [26] J. Ho Kim, J. Franck, T. Kang, H. Heinsen, R. Ravid, I. Ferrer, M. Hee Cheon, J.-Y. Lee, J. Shin Yoo, H.W. Steinbusch, M. Salzet, I. Fournier, Y. Mok Park, Proteome-wide characterization of signalling interactions in the hippocampal CA4/DG subfield of patients with Alzheimer’s disease, *Sci. Rep.* 5 (2015) 11138. doi:10.1038/srep11138.
- [27] K. Huber, M. Aichler, N. Sun, A. Buck, Z. Li, I.E. Fernandez, S.M. Hauck, H. Zitzelsberger, O. Eickelberg, K.P. Janssen, U. Keller, A. Walch, A rapid ex vivo tissue model for optimising

- drug detection and ionisation in MALDI imaging studies, *Histochem. Cell Biol.* 142 (2014) 361–371. doi:10.1007/s00418-014-1223-0.
- [28] J.G. Swales, J.W. Tucker, M.J. Spreadborough, S.L. Iverson, M.R. Clench, P.J.H. Webborn, R.J.A. Goodwin, Mapping Drug Distribution in Brain Tissue Using Liquid Extraction Surface Analysis Mass Spectrometry Imaging, *Anal. Chem.* 87 (2015) 10146–10152. doi:10.1021/acs.analchem.5b02998.
- [29] H. Aikawa, M. Hayashi, S. Ryu, M. Yamashita, N. Ohtsuka, M. Nishidate, Y. Fujiwara, A. Hamada, Visualizing spatial distribution of alectinib in murine brain using quantitative mass spectrometry imaging, *Sci. Rep.* 6 (2016) 23749. doi:10.1038/srep23749.
- [30] B. Prideaux, M. Stoeckli, Mass spectrometry imaging for drug distribution studies, *J. Proteomics.* 75 (2012) 4999–5013. doi:10.1016/j.jprot.2012.07.028.
- [31] B. Prideaux, L.E. Via, M.D. Zimmerman, S. Eum, J. Sarathy, P. O'Brien, C. Chen, F. Kaya, D.M. Weiner, P.-Y. Chen, T. Song, M. Lee, T.S. Shim, J.S. Cho, W. Kim, S.N. Cho, K.N. Olivier, C.E. Barry, V. Dartois, The association between sterilizing activity and drug distribution into tuberculosis lesions, *Nat. Med.* 21 (2015) 1223–1227. doi:10.1038/nm.3937.
- [32] R.M. Caprioli, T.B. Farmer, J. Gile, Molecular imaging of biological samples: localization of peptides and proteins using MALDI-TOF MS, *Anal. Chem.* 69 (1997) 4751–4760.
- [33] B. Cillero-Pastor, G.B. Eijkel, F.J. Blanco, R.M.A. Heeren, Protein classification and distribution in osteoarthritic human synovial tissue by matrix-assisted laser desorption ionization mass spectrometry imaging, *Anal. Bioanal. Chem.* 407 (2015) 2213–2222. doi:10.1007/s00216-014-8342-2.
- [34] A.S. Attia, K.A. Schroeder, E.H. Seeley, K.J. Wilson, N.D. Hammer, D.C. Colvin, M.L. Manier, J.J. Nicklay, K.L. Rose, J.C. Gore, R.M. Caprioli, E.P. Skaar, Monitoring the inflammatory response to infection through the integration of MALDI IMS and MRI, *Cell Host Microbe.* 11 (2012) 664–673. doi:10.1016/j.chom.2012.04.018.
- [35] H. Hirano, N. Masaki, T. Hayasaka, Y. Watanabe, K. Masumoto, T. Nagata, F. Katou, M. Setou, Matrix-assisted laser desorption/ionization imaging mass spectrometry revealed traces of dental problem associated with dental structure, *Anal. Bioanal. Chem.* 406 (2014) 1355–1363. doi:10.1007/s00216-013-7075-y.
- [36] O. Klein, K. Strohschein, G. Nebrich, J. Oetjen, D. Trede, H. Thiele, T. Alexandrov, P. Giavalisco, G.N. Duda, P. von Roth, S. Geissler, J. Klose, T. Winkler, MALDI imaging mass spectrometry: Discrimination of pathophysiological regions in traumatized skeletal muscle by characteristic peptide signatures, *PROTEOMICS.* 14 (2014) 2249–2260. doi:10.1002/pmic.201400088.
- [37] A. Roux, L. Muller, S.N. Jackson, J. Post, K. Baldwin, B. Hoffer, C.D. Balaban, D. Barbacci, J.A. Schultz, S. Gouty, B.M. Cox, A.S. Woods, Mass spectrometry imaging of rat brain lipid profile changes over time following traumatic brain injury, *J. Neurosci. Methods.* 272 (2016) 19–32. doi:10.1016/j.jneumeth.2016.02.004.
- [38] L. Mourino-Alvarez, I. Iloro, F. de la Cuesta, M. Azkargorta, T. Sastre-Oliva, I. Escobes, L.F. Lopez-Almodovar, P.L. Sanchez, H. Urreta, F. Fernandez-Aviles, A. Pinto, L.R. Padial, F. Akerström, F. Elortza, M.G. Barderas, MALDI-Imaging Mass Spectrometry: a step forward in the anatomopathological characterization of stenotic aortic valve tissue, *Sci. Rep.* 6 (2016) 27106. doi:10.1038/srep27106.
- [39] E. Acquadro, I. Caron, M. Tortarolo, E.M. Bucci, C. Bendotti, D. Corpillo, Human SOD1-G93A specific distribution evidenced in murine brain of a transgenic model for amyotrophic lateral sclerosis by MALDI imaging mass spectrometry, *J. Proteome Res.* 13 (2014) 1800–1809. doi:10.1021/pr400942n.
- [40] J. Kriegsmann, M. Kriegsmann, R. Casadonte, MALDI TOF imaging mass spectrometry in clinical pathology: a valuable tool for cancer diagnostics (review), *Int. J. Oncol.* 46 (2015) 893–906. doi:10.3892/ijo.2014.2788.

- [41] R. Longuespée, R. Casadonte, M. Kriegsmann, C. Pottier, G. Picard de Muller, P. Delvenne, J. Kriegsmann, E. De Pauw, MALDI mass spectrometry imaging: A cutting-edge tool for fundamental and clinical histopathology, *Proteomics Clin. Appl.* 10 (2016) 701–719. doi:10.1002/prca.201500140.
- [42] S. Koizumi, S. Yamamoto, T. Hayasaka, Y. Konishi, M. Yamaguchi-Okada, N. Goto-Inoue, Y. Sugiura, M. Setou, H. Namba, Imaging mass spectrometry revealed the production of lyso-phosphatidylcholine in the injured ischemic rat brain, *Neuroscience*. 168 (2010) 219–225. doi:10.1016/j.neuroscience.2010.03.056.
- [43] H.-Y.J. Wang, H.-W. Wu, P.-J. Tsai, C.B. Liu, MALDI-mass spectrometry imaging of desalted rat brain sections reveals ischemia-mediated changes of lipids, *Anal. Bioanal. Chem.* 404 (2012) 113–124. doi:10.1007/s00216-012-6077-5.
- [44] S.R. Shanta, C.S. Choi, J.H. Lee, C.Y. Shin, Y.J. Kim, K.-H. Kim, K.P. Kim, Global changes in phospholipids identified by MALDI MS in rats with focal cerebral ischemia, *J. Lipid Res.* 53 (2012) 1823–1831. doi:10.1194/jlr.M022558.
- [45] J.A. Vizcaíno, E.W. Deutsch, R. Wang, A. Csordas, F. Reisinger, D. Ríos, J.A. Dienes, Z. Sun, T. Farrah, N. Bandeira, P.-A. Binz, I. Xenarios, M. Eisenacher, G. Mayer, L. Gatto, A. Campos, R.J. Chalkley, H.-J. Kraus, J.P. Albar, S. Martinez-Bartolomé, R. Apweiler, G.S. Omenn, L. Martens, A.R. Jones, H. Hermjakob, ProteomeXchange provides globally coordinated proteomics data submission and dissemination, *Nat. Biotechnol.* 32 (2014) 223–226. doi:10.1038/nbt.2839.
- [46] M.R. Wilkins, I. Lindskog, E. Gasteiger, A. Bairoch, J.C. Sanchez, D.F. Hochstrasser, R.D. Appel, Detailed peptide characterization using PEPTIDEMASS—a World-Wide-Web-accessible tool, *Electrophoresis*. 18 (1997) 403–408. doi:10.1002/elps.1150180314.
- [47] M.M. Gessel, J.L. Norris, R.M. Caprioli, MALDI imaging mass spectrometry: spatial molecular analysis to enable a new age of discovery, *J. Proteomics*. 107 (2014) 71–82. doi:10.1016/j.jprot.2014.03.021.
- [48] J. Hanrieder, A. Ljungdahl, M. Fälth, S.E. Mammo, J. Bergquist, M. Andersson, L-DOPA-induced Dyskinesia is Associated with Regional Increase of Striatal Dynorphin Peptides as Elucidated by Imaging Mass Spectrometry, *Mol. Cell. Proteomics*. 10 (2011) M111.009308. doi:10.1074/mcp.M111.009308.
- [49] A. Ljungdahl, J. Hanrieder, M. Fälth, J. Bergquist, M. Andersson, Imaging Mass Spectrometry Reveals Elevated Nigral Levels of Dynorphin Neuropeptides in L-DOPA-Induced Dyskinesia in Rat Model of Parkinson's Disease, *PLoS ONE*. 6 (2011). doi:10.1371/journal.pone.0025653.
- [50] H.C. Diehl, B. Beine, J. Elm, D. Trede, M. Ahrens, M. Eisenacher, K. Marcus, H.E. Meyer, C. Henkel, The challenge of on-tissue digestion for MALDI MSI- a comparison of different protocols to improve imaging experiments, *Anal. Bioanal. Chem.* 407 (2015) 2223–2243. doi:10.1007/s00216-014-8345-z.
- [51] J.M. Spraggins, D.G. Rizzo, J.L. Moore, K.L. Rose, N.D. Hammer, E.P. Skaar, R.M. Caprioli, MALDI FTICR IMS of Intact Proteins: Using Mass Accuracy to Link Protein Images with Proteomics Data, *J. Am. Soc. Mass Spectrom.* 26 (2015) 974–985. doi:10.1007/s13361-015-1147-5.
- [52] J.M. Spraggins, D.G. Rizzo, J.L. Moore, M.J. Noto, E.P. Skaar, R.M. Caprioli, Next-generation technologies for spatial proteomics: Integrating ultra-high speed MALDI-TOF and high mass resolution MALDI FTICR imaging mass spectrometry for protein analysis, *Proteomics*. 16 (2016) 1678–1689. doi:10.1002/pmic.201600003.
- [53] Y. Terasaki, Y. Liu, K. Hayakawa, L.D. Pham, E.H. Lo, X. Ji, K. Arai, Mechanisms of neurovascular dysfunction in acute ischemic brain, *Curr. Med. Chem.* 21 (2014) 2035–2042.
- [54] R.A. Floyd, R.A. Towner, T. He, K. Hensley, K.R. Maples, Translational research involving oxidative stress and diseases of aging, *Free Radic. Biol. Med.* 51 (2011) 931–941. doi:10.1016/j.freeradbiomed.2011.04.014.

- [55] A. Gaballo, F. Zanotti, S. Papa, Structures and interactions of proteins involved in the coupling function of the protonmotive F_oF₁-ATP synthase, *Curr. Protein Pept. Sci.* 3 (2002) 451–460.
- [56] I. Rutkai, P.V.G. Katakam, S. Dutta, D.W. Busija, Sustained mitochondrial functioning in cerebral arteries after transient ischemic stress in the rat: a potential target for therapies, *Am. J. Physiol. Heart Circ. Physiol.* 307 (2014) H958–966. doi:10.1152/ajpheart.00405.2014.
- [57] J.-W. Seo, Y. Kim, J. Hur, K.-S. Park, Y.-W. Cho, Proteomic analysis of primary cultured rat cortical neurons in chemical ischemia, *Neurochem. Res.* 38 (2013) 1648–1660. doi:10.1007/s11064-013-1067-3.
- [58] B. Kadenbach, M. Hüttemann, The subunit composition and function of mammalian cytochrome c oxidase, *Mitochondrion.* 24 (2015) 64–76. doi:10.1016/j.mito.2015.07.002.
- [59] S.J. Kish, F. Mastrogiacomo, M. Guttman, Y. Furukawa, J.W. Taanman, S. Dozić, M. Pandolfo, J. Lamarche, L. DiStefano, L.J. Chang, Decreased brain protein levels of cytochrome oxidase subunits in Alzheimer’s disease and in hereditary spinocerebellar ataxia disorders: a nonspecific change?, *J. Neurochem.* 72 (1999) 700–707.
- [60] V. Borutaite, A. Toleikis, G.C. Brown, In the eye of the storm: mitochondrial damage during heart and brain ischaemia, *FEBS J.* 280 (2013) 4999–5014. doi:10.1111/febs.12353.
- [61] W. Yin, A.P. Signore, M. Iwai, G. Cao, Y. Gao, J. Chen, Rapidly increased neuronal mitochondrial biogenesis after hypoxic-ischemic brain injury, *Stroke J. Cereb. Circ.* 39 (2008) 3057–3063. doi:10.1161/STROKEAHA.108.520114.
- [62] Y. Xie, J. Li, G. Fan, S. Qi, B. Li, Reperfusion promotes mitochondrial biogenesis following focal cerebral ischemia in rats, *PloS One.* 9 (2014) e92443. doi:10.1371/journal.pone.0092443.
- [63] V.M. Selaković, M.D. Jovanović, R.R. Mihajlović, L.L.J. Radenović, Dynamics of cytochrome c oxidase activity in acute ischemic stroke, *Acta Neurol. Scand.* 111 (2005) 329–332. doi:10.1111/j.1600-0404.2005.00403.x.
- [64] Y. Takahashi, T. Sugawara, T. Miyazaki, H. Itoh, K. Mizoi, Aberrant increase in cytochrome c oxidase subunit I precedes neuronal death after cerebral ischemia, *Neuroreport.* 24 (2013) 872–877. doi:10.1097/WNR.000000000000018.
- [65] W. Liu, F. Tian, T. Kurata, N. Morimoto, K. Abe, Dynamic changes of mitochondrial fission proteins after transient cerebral ischemia in mice, *Brain Res.* 1456 (2012) 94–99. doi:10.1016/j.brainres.2012.03.038.
- [66] T.H. Sanderson, C.A. Reynolds, R. Kumar, K. Przyklenk, M. Hüttemann, Molecular mechanisms of ischemia-reperfusion injury in brain: pivotal role of the mitochondrial membrane potential in reactive oxygen species generation, *Mol. Neurobiol.* 47 (2013) 9–23. doi:10.1007/s12035-012-8344-z.
- [67] W. Aulbert, K. Weigt-Usinger, C. Thiels, C. Köhler, M. Vorgerd, A. Schreiner, S. Hoffjan, T. Rothoef, S.B. Wortmann, C.M. Heyer, T. Podskarbi, T. Lücke, Long survival in Leigh syndrome: new cases and review of literature, *Neuropediatrics.* 45 (2014) 346–353. doi:10.1055/s-0034-1383823.
- [68] F. Baertling, M. A M van den Brand, J.L. Hertecant, A. Al-Shamsi, L. P van den Heuvel, F. Distelmaier, E. Mayatepek, J.A. Smeitink, L.G.J. Nijtmans, R.J.T. Rodenburg, Mutations in COA6 cause cytochrome c oxidase deficiency and neonatal hypertrophic cardiomyopathy, *Hum. Mutat.* 36 (2015) 34–38. doi:10.1002/humu.22715.
- [69] V. Massa, E. Fernandez-Vizarrá, S. Alshahwan, E. Bakhsh, P. Goffrini, I. Ferrero, P. Mereghetti, P. D’Adamo, P. Gasparini, M. Zeviani, Severe infantile encephalomyopathy caused by a mutation in COX6B1, a nucleus-encoded subunit of cytochrome c oxidase, *Am. J. Hum. Genet.* 82 (2008) 1281–1289. doi:10.1016/j.ajhg.2008.05.002.
- [70] D. Lee, K.-Y. Kim, Y.H. Noh, S. Chai, J.D. Lindsey, M.H. Ellisman, R.N. Weinreb, W.-K. Ju, Brimonidine blocks glutamate excitotoxicity-induced oxidative stress and preserves

- mitochondrial transcription factor a in ischemic retinal injury, *PLoS One*. 7 (2012) e47098. doi:10.1371/journal.pone.0047098.
- [71] V. Procaccio, C. Bris, J.M. Chao de la Barca, F. Oca, A. Chevrollier, P. Amati-Bonneau, D. Bonneau, P. Reynier, Perspectives of drug-based neuroprotection targeting mitochondria, *Rev. Neurol. (Paris)*. 170 (2014) 390–400. doi:10.1016/j.neurol.2014.03.005.
- [72] A.R. Van Rompay, M. Johansson, A. Karlsson, Phosphorylation of nucleosides and nucleoside analogs by mammalian nucleoside monophosphate kinases, *Pharmacol. Ther.* 87 (2000) 189–198.
- [73] J.-Y. Liou, G.E. Dutschman, W. Lam, Z. Jiang, Y.-C. Cheng, Characterization of human UMP/CMP kinase and its phosphorylation of D- and L-form deoxycytidine analogue monophosphates, *Cancer Res.* 62 (2002) 1624–1631.
- [74] M. Cansev, Uridine and cytidine in the brain: their transport and utilization, *Brain Res. Rev.* 52 (2006) 389–397. doi:10.1016/j.brainresrev.2006.05.001.
- [75] H. Onodera, K. Iijima, K. Kogure, Mononucleotide metabolism in the rat brain after transient ischemia, *J. Neurochem.* 46 (1986) 1704–1710.
- [76] O. Carrette, J.A. Burgess, P.R. Burkhard, C. Lang, M. Côte, N. Rodrigo, D.F. Hochstrasser, J.-C. Sanchez, Changes of the cortex proteome and Apolipoprotein E in transgenic mouse models of Alzheimer's Disease, *J. Chromatogr. B Analyt. Technol. Biomed. Life. Sci.* 840 (2006) 1–9. doi:10.1016/j.jchromb.2006.05.019.
- [77] J.D. Pallua, G. Schaefer, C. Seifarth, M. Becker, S. Meding, S. Rauser, A. Walch, M. Handler, M. Netzer, M. Popovscaia, M. Osl, C. Baumgartner, H. Lindner, L. Kremser, B. Sarg, G. Bartsch, C.W. Huck, G.K. Bonn, H. Klocker, MALDI-MS tissue imaging identification of biliverdin reductase B overexpression in prostate cancer, *J. Proteomics.* 91 (2013) 500–514. doi:10.1016/j.jprot.2013.08.003.
- [78] M. Martin-Lorenzo, B. Balluff, A.S. Maroto, R.J. Carreira, R.J.M. van Zeijl, L. Gonzalez-Calero, F. de la Cuesta, M.G. Barderas, L.F. Lopez-Almodovar, L.R. Padial, L.A. McDonnell, F. Vivanco, G. Alvarez-Llamas, Molecular anatomy of ascending aorta in atherosclerosis by MS Imaging: Specific lipid and protein patterns reflect pathology, *J. Proteomics.* 126 (2015) 245–251. doi:10.1016/j.jprot.2015.06.005.

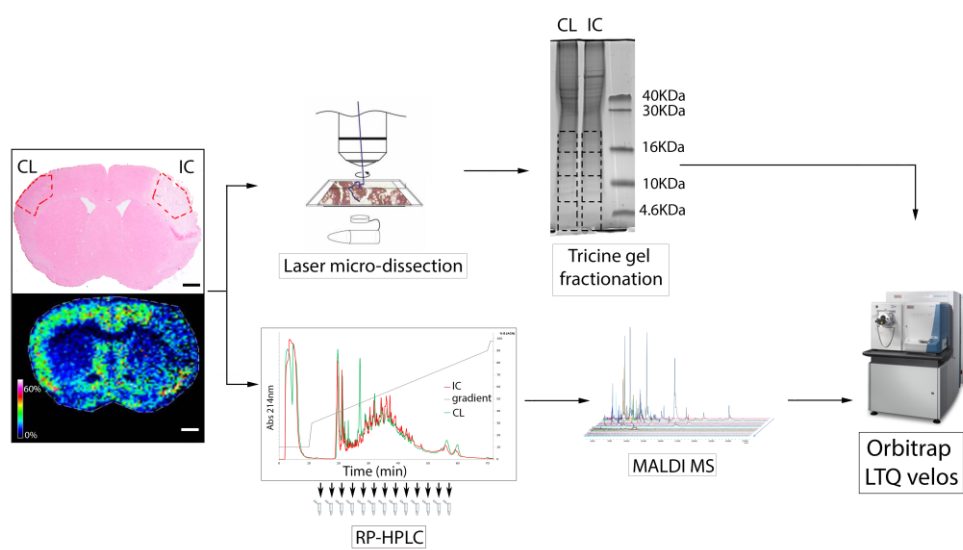


Figure 1

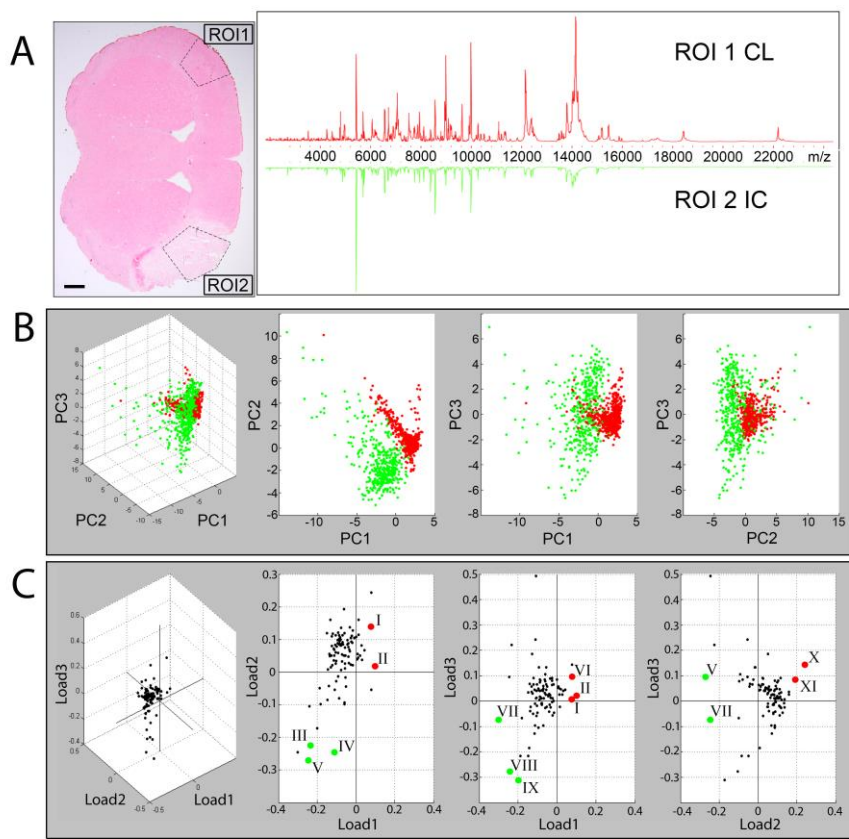


Figure 2

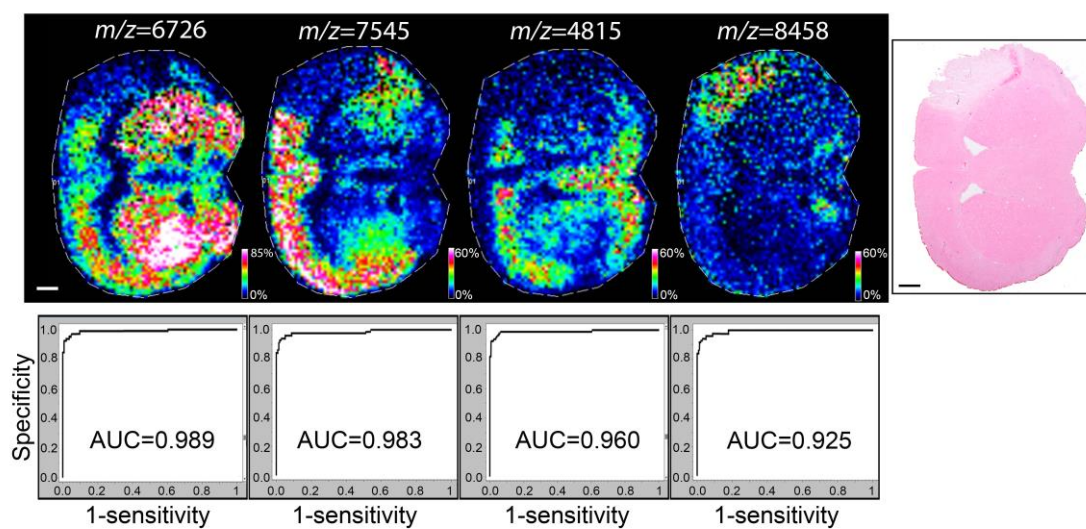


Figure 3

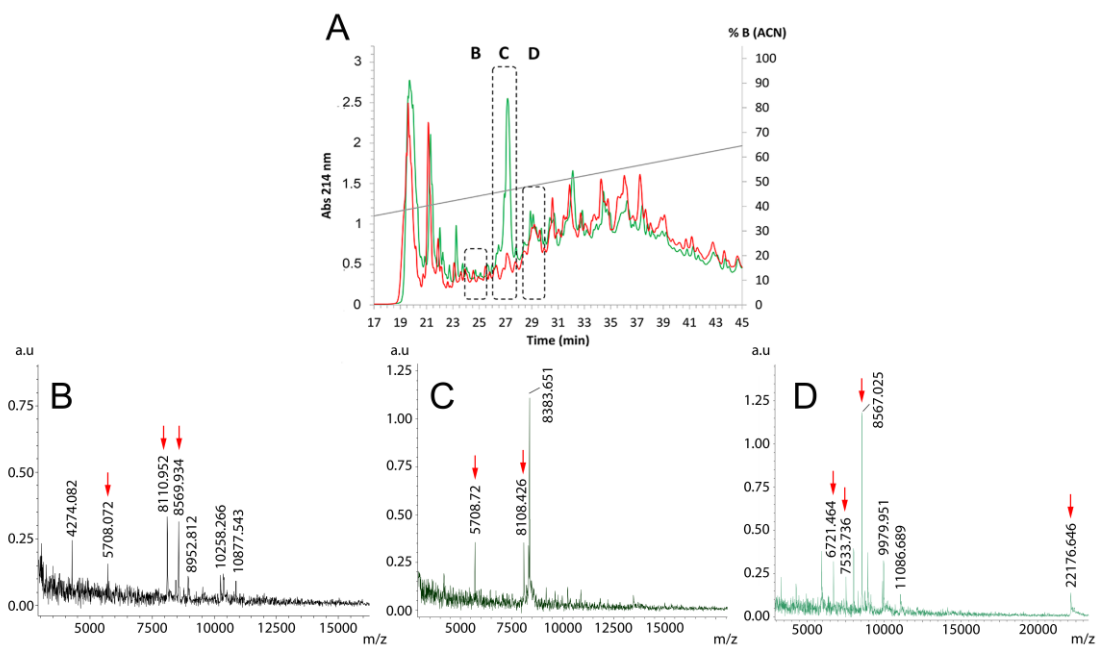


Figure 4

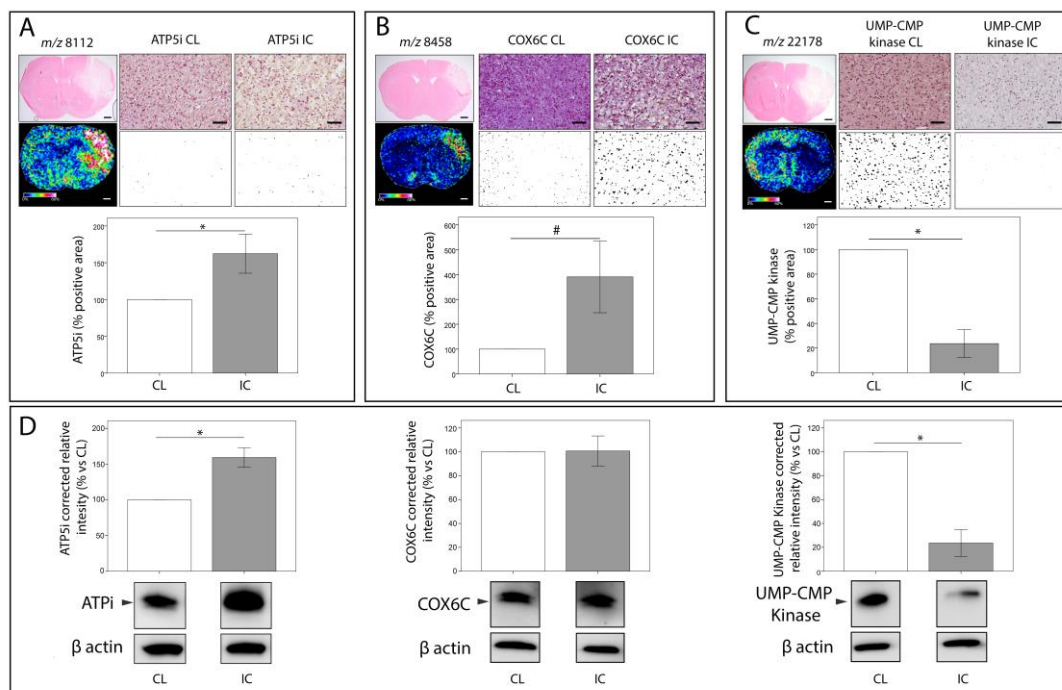
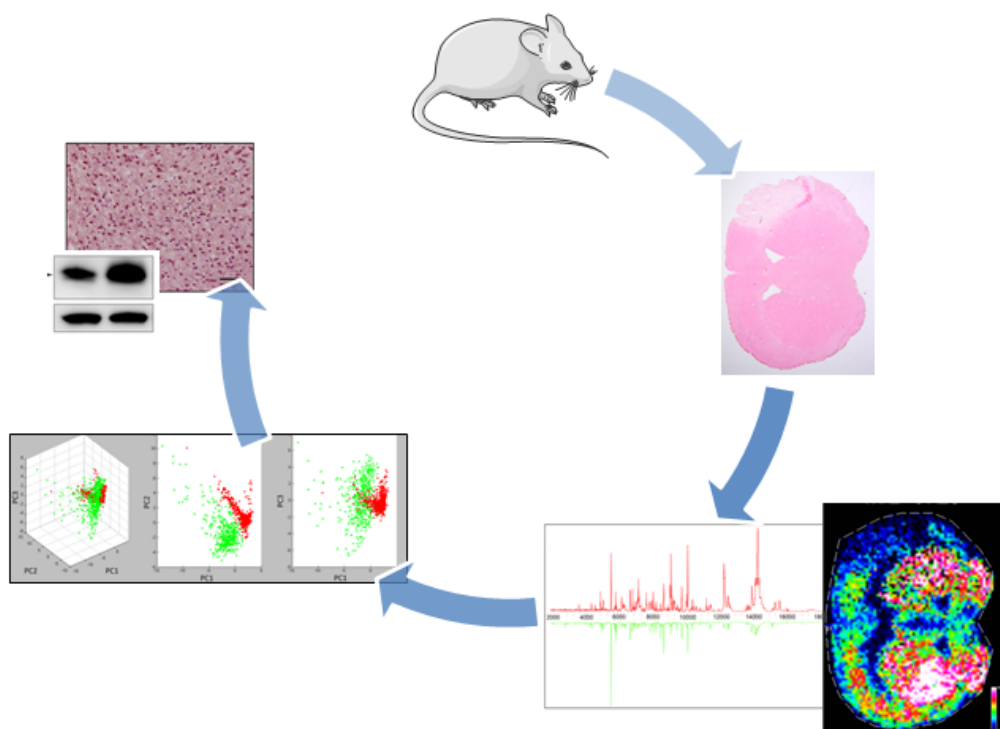


Figure 5



Graphical abstract

ACCEPTED

Funding sources

Neurovascular Research Laboratory takes part into the Spanish stroke research network INVICTUS (RD12/0014/0005) and is partially funded by grants from the Fondo de Investigaciones Sanitarias (PI11/00176), Instituto de Salud Carlos III. VHIO Proteomics Laboratory is a member of Proteored, PRB2-ISCIII and is supported by grant PT13/0001, of the PE I+D+i 2013-2016, funded by Instituto de Salud Carlos III. M. Hernández-Guillamon is supported by the Miquel Servet programme (CP12/0359) and A. Rosell is supported by the Miguel Servet program (CPII15/00003), both from the Instituto de Salud Carlos III. A. Simats holds a predoctoral fellowship (2015 FI_B 00952) from the AGAUR. F. Ma is supported by a predoctoral Fellowship from the China Scholarship Council. Several of these research programs are co-financed by the European Regional Development Fund (ERDF).

Notes

All authors declare no conflict of interest.

Significance: We identified for the first time using MALDI-IMS new proteins that might be involved in brain ischemia representing potential diagnostic biomarkers or target molecules for neurological recovery.

ACCEPTED MANUSCRIPT

Highlights

- We performed a protein profile analysis of brain tissue subjected to ischemia.
- We identified protein species (m/z values) involved in brain ischemia using two different identification approaches.
- A novel strategy was carried out to match m/z with protein molecular weights.
- Identified proteins represent potential biomarkers/therapeutic targets for neurological recovery after cerebral ischemia.

ACCEPTED MANUSCRIPT